Icarus 408 (2024) 115800

Contents lists available at ScienceDirect

Icarus

journal homepage: www.elsevier.com/locate/icarus

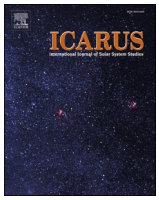

Characterization of aqueous alteration and formation of salty exposures at Ius Chasma, Mars

Kierra A. Wilk [a,*], Janice L. Bishop [b], Catherine M. Weitz [c], Mario Parente [d], Arun M. Saranathan [d], Yuki Itoh [d,e], Christoph Gross [f], Jessica Flahaut [g], Frank Seelos [e]

[a] Department of Earth, Environmental, and Planetary Sciences, Brown University, Providence, RI 02912, United States
[b] SETI Institute & NASA-Ames, Mountain View, CA, United States
[c] Planetary Science Institute, Tucson, AZ, United States
[d] University of Massachusetts at Amherst, Amherst, MA, United States
[e] Johns Hopkins University Applied Physics Lab, Laurel, MD, United States
[f] Free University of Berlin, Berlin, Germany
[g] CRPG, CNRS/Université de Lorraine, Vandœuvre-lès-Nancy, France

ARTICLE INFO

Keywords:
Mars
Mars surface
Spectroscopy

ABSTRACT

Intriguing outcrops in Ius Chasma provide a window into past aqueous processes in Valles Marineris, Mars. Hydrous sulfate minerals are abundant throughout this region, but one area in Ius Chasma includes phyllosilicates, opal, and additional materials with unusual spectral features. This study at Geryon Montes, an east-west horst that divides Ius Chasma into a northern and southern canyon, exploits recent advances in image calibration and feature extraction techniques for analysis of hyperspectral images acquired by the Compact Reconnaissance Imaging Spectrometer for Mars (CRISM). Specifically, a unique spectral "doublet" feature with absorptions at 2.21–2.23 and 2.26–2.28 μm is isolated at the border of phyllosilicate-bearing and sulfate-bearing regions in Ius Chasma and surveyed to characterize outcrops that may represent a changing climate on Mars. We document and map three distinct forms of this "doublet" material in relation to phyllosilicates and opal. Analyses of compositional maps derived from CRISM overlain on High Resolution Stereo Camera (HRSC) and High Resolution Imaging Science Experiment (HiRISE) imagery has revealed the presence of these hydrated outcrops along the wall rocks below a breach in the Geryon Montes, bordering a canyon containing abundant hydrated sulfates. Our investigation supports formation of these unique alteration phases through acid alteration of ancient smectites in the wall rock as the sulfate brine overflowed the south canyon of Ius Chasma at the breach in Geryon Montes and penetrated the deeper northern canyon.

1. Introduction

Valles Marineris extends over ~ 4000 km along the Martian equator, exposing a wide variety of mineralogy ranging from basaltic components to sulfates and phyllosilicates. The complex canyon system (Fueten et al., 2014) formed after the accumulation of lavas that were part of the Tharsis volcanism (Tanaka, 1986; Tanaka et al., 1991) and include Noachian-aged ancestral basins (Lucchitta and Bertolini, 1990; Lucchitta et al., 1994) that were reshaped during the Hesperian to the current structure (Scott and Tanaka, 1986; Tanaka, 1986; Dohm and Tanaka, 1999; Head et al., 2001; Carr and Head, 2010) and modified with faulting and linear troughs in the Amazonian (Schultz, 1998). Water has also played an important role in shaping (Sivasankari and Arivazhagan, 2022) and creating alteration products and sediments within Valles Marineris (Gendrin et al., 2005; Chojnacki and Hynek, 2008; Murchie et al., 2009a).

Throughout the Valles Marineris region, light-toned layered deposits have been observed along the plateaus by the Mars Reconnaissance Orbiter (MRO) HiRISE (McEwen et al., 2007) and CRISM (S. L. Murchie et al., 2007) instruments west of Ganges Chasma, southwest of Melas Chasma, south of western Candor Chasma, northwest of Juventae Chasma, south of Ius Chasma (Weitz et al., 2010) and south of Coprates and Capri Chasmata (Le Deit et al., 2012). These light-toned layered deposits are associated with valley or channel systems, with three of the

* Corresponding author.
E-mail address: kierra_wilk@brown.edu (K.A. Wilk).

https://doi.org/10.1016/j.icarus.2023.115800
Received 27 February 2023; Received in revised form 25 August 2023; Accepted 13 September 2023
Available online 22 September 2023

deposits (Juventae, Ius, and Ganges Chasma) having inverted channels made of light-toned beds (Weitz et al., 2010). Within the canyons of Valles Marineris, thicker mounds of light-toned layered deposits are spectrally dominated by hydrated sulfates, including monohydrated sulfates (MHS) and polyhydrated sulfates (PHS) visible at km scales in the Mars Express Observatoire pour la Mineralogie, l'Eau, les Glaces et l'Activité (OMEGA) (Gendrin et al., 2005; Bibring et al., 2006) and MRO/CRISM data (e.g. Murchie et al., 2009a). Horizons of PHS and MHS units, sometimes alternating but frequently with PHS above MHS, have been observed in many of the chasmata across Valles Marineris and nearby including Candor Chasma (Murchie et al., 2009b; Roach et al., 2009; Fueten et al., 2014), Capri Chasma (Flahaut et al., 2010; Weitz et al., 2012), and Juventae Chasma (Bishop et al., 2009; Noel et al., 2015; Fueten et al., 2017).

Orbital characterization of the unique light-toned outcrops on Mars using CRISM data indicate broader geochemical transitions from sedimentary phyllosilicate beds to evaporative, acidic, or hydrothermal environments containing sulfate minerals (e.g. Bibring et al., 2006). Several thin outcrops have been identified on Mars using a spectral "doublet" feature with two absorption bands between 2.2 and 2.3 μm at multiple locations including Mawrth Vallis (Bishop et al., 2020), Noctis Labyrinthus (Weitz et al., 2011), Melas Chasma (Weitz et al., 2015), Coprates Catena (Weitz and Bishop, 2016), and Ius Chasma (Roach et al., 2010). The "doublet" type units at Mawrth Vallis are sandwiched in between Al-phyllosilicates and Fe/Mg-smectites in expansive clay beds and in some cases, small pockets of jarosite are observed in or adjacent to the "doublet" materials (Bishop et al., 2020). Noctis Labyrinthus, adjoined to the westernmost chasmata of Valles Marineris, is known for mineralogic diversity with outcrops containing multiple aqueous minerals (Weitz et al., 2011; Thollot et al., 2012) and also this "doublet" signature (Weitz et al., 2011). The spectral "doublet" units observed at Melas Chasma occur in smaller outcrops along the upper wall rock slopes in far western Melas adjacent to Ius Chasma (Weitz et al., 2015). This study builds on these previous orbital studies of the doublet materials and spectral analyses of analog sites containing phyllosilicate-sulfate assemblages (Bishop et al., 2015; Bishop and Murad, 2005)(Kaplan et al., 2016; Perrin et al., 2018a)(Bishop et al., 2019). Here we focus on Ius Chasma (Fig. 1), which contains perhaps the most intriguing "doublet" type units, as they form a continuous thin sloped layer that spans tens of kilometers.

Previous work (Roach et al., 2010; Kaplan et al., 2016) investigated these enigmatic "doublet" materials found in the light-toned layered deposits at Ius Chasma that span hundreds of kilometers. The "doublet" materials are emplaced on top of Fe/Mg smectites, and their origin has been interpreted as being either an acid-leached phyllosilicate from the underlying unit, or as a smectite/jarosite mixture (Roach et al., 2010). Analysis of spectral and mineralogical analogs from Rio Tinto led Kaplan et al. (2016) suggest that the "doublet" material is consistent with an Al-phyllosilicate and jarosite mixture due to the independently varying strength of the doublet feature, the similarity in the spectral doublet wavelength positions seen at both Rio Tinto and on Mars, and the wavelength positions of the spectral doublet feature being somewhat consistent with Al-OH and Fe-OH bearing minerals.

Itoh and Parente (2021) recently proposed a new atmospheric

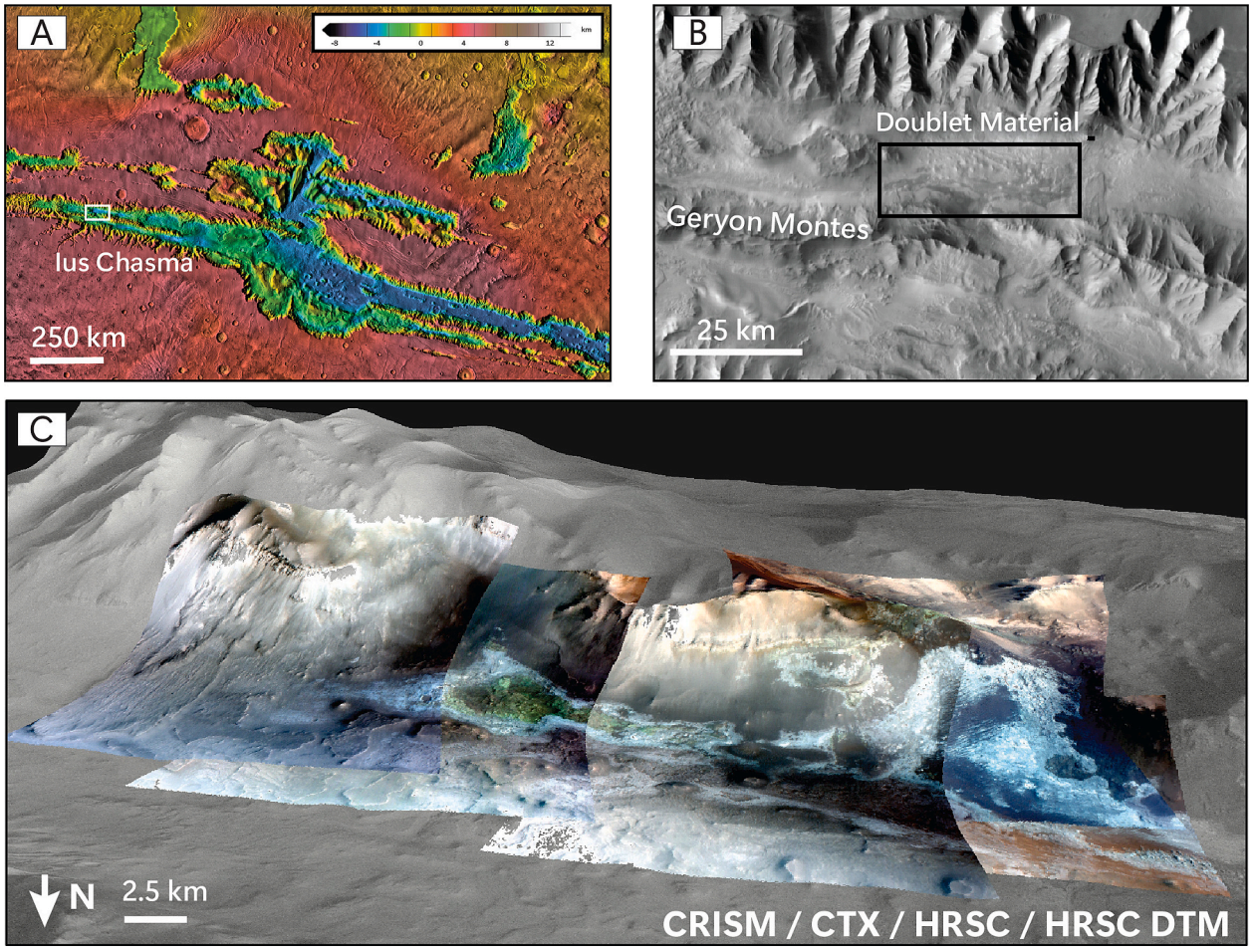

Fig. 1. (A) MOLA image of Valles Marineris, including Ius Chasma. (B) THEMIS Day IR image of Ius Chasma including Geryon Montes and the bright layered materials containing the "doublet" spectral signatures. (C) HRSC DTM overlain by CTX and CRISM images of the doublet type unit on the southern wall of the northern valley of Ius Chasma.

correction and de-noising algorithm, SUBCONV, for CRISM IR images that significantly mitigates atmospheric residuals and spurious features, clarifying surface spectral features. Furthermore, Saranathan and Parente, 2021 developed novel feature extracting algorithms that allow for the isolation and mapping of unique image components using the CRISM images processed by the SUBCONV algorithm. The advancement of the improved CRISM image processing and mineral mapping techniques enables the characterization of smaller outcrops that were previously difficult to resolve.

The objectives of our study are to reinvestigate these intriguing spectral "doublet" outcrops near Geryon Montes in Ius Chasma through coordinated analyses of compositional information from CRISM and morphology and stratigraphy from HiRISE and the Mars Express High Resolution Stereo Camera (HRSC). Our analysis includes a high level CRISM product set, the Map-Projected Targeted Reduced Data Records (MTRDR) (Seelos et al., 2023), processed and released by the CRISM Science Operation Center, though we are primarily employing the newer SUBCONV image processing technique that offers improved clarity of CRISM images with reduced noise and improved spectral features of surface outcrops, coupled with the new feature extraction algorithm to map out spectrally distinct components in these scenes. We are using these techniques to explore the types of minerals and other components that best explain the doublet features and to assess how these intriguing deposits formed at Ius Chasma.

2. Methods

This study focuses on visible/near-infrared (VNIR) spectral image cubes acquired by the CRISM instrument in the Full Resolution Targeted (FRT) observation mode that nominally achieves the spatial resolution of 18 m/pixel. We made use of the I/F image cubes of the MTRDR products (Seelos et al., 2023) that were already photometrically and atmospherically corrected and map projected. Some of the remaining residuals in the I/F spectra in the MTRDR product are mitigated by ratioing spectra from areas of interest to spectrally neutral sites in the image. Spectral parameters (Viviano et al., 2014) were further used to identify and map individual mineral units in complex outcrops in CRISM scenes. ArcGIS software was then used to overlay CRISM maps of specific minerals (e.g., Bishop et al., 2020) on imagery collected by HiRISE, the Context (CTX) camera onboard MRO and HRSC digital terrain models (DTM).

For this study we are also using CRISM images prepared with the new SUBCONV algorithm developed by Itoh and Parente (2021) for simultaneous atmospheric correction and denoising processed using the older TRDR-equivalent I/F data produced by our own implementation of the TRDR version 3 calibration pipeline excluding bad-pixel interpolation and TRR3 filtering. Images processed using this new method are free of most of the residual of the atmospheric correction from the volcano scan method, as well as large noise and spurious artifacts that would mask or mimic surface spectral signatures in the 1.0–2.6 μm spectral range. Spectra of selected "doublet" units were analyzed from images processed with both methods to ensure consistency (Fig. 2).

We processed images containing a "doublet" feature using a new feature extracting algorithm (Saranathan and Parente, 2021) based on Generative Adversarial Networks (GANs). GANs are a class of neural network models, called generative models designed to learn and mimic the patterns/modalities of a specific dataset. Given their ability to learn the various intricacies of a specific dataset from unlabeled samples, they have been successfully used as feature extractors to improve the performance of classification (Zhang et al., 2018) and mapping algorithms (Saranathan and Parente, 2021) for hyperspectral datasets. The GAN-based mapping has proven to be effective in identifying and mapping the boundaries of mineral deposits in CRISM images. In this study, the various images were mapped using a base set (of well-known mineral shapes known to be present in the CRISM image database) and manually selected CRISM spectra representing the most distinct "doublet" type units. The base set of minerals used in the mapping are shown in Table 1, these spectral shapes are drawn from the CRISM MICA Spectral Library (Viviano et al., 2014). Additionally, we are mapping subtle differences in the "doublet" materials and associated minerals in relation to neighboring outcrops using hyperspectral factors (i.e., slope, absorption features, etc., see Saranathan and Parente, 2021) between 1

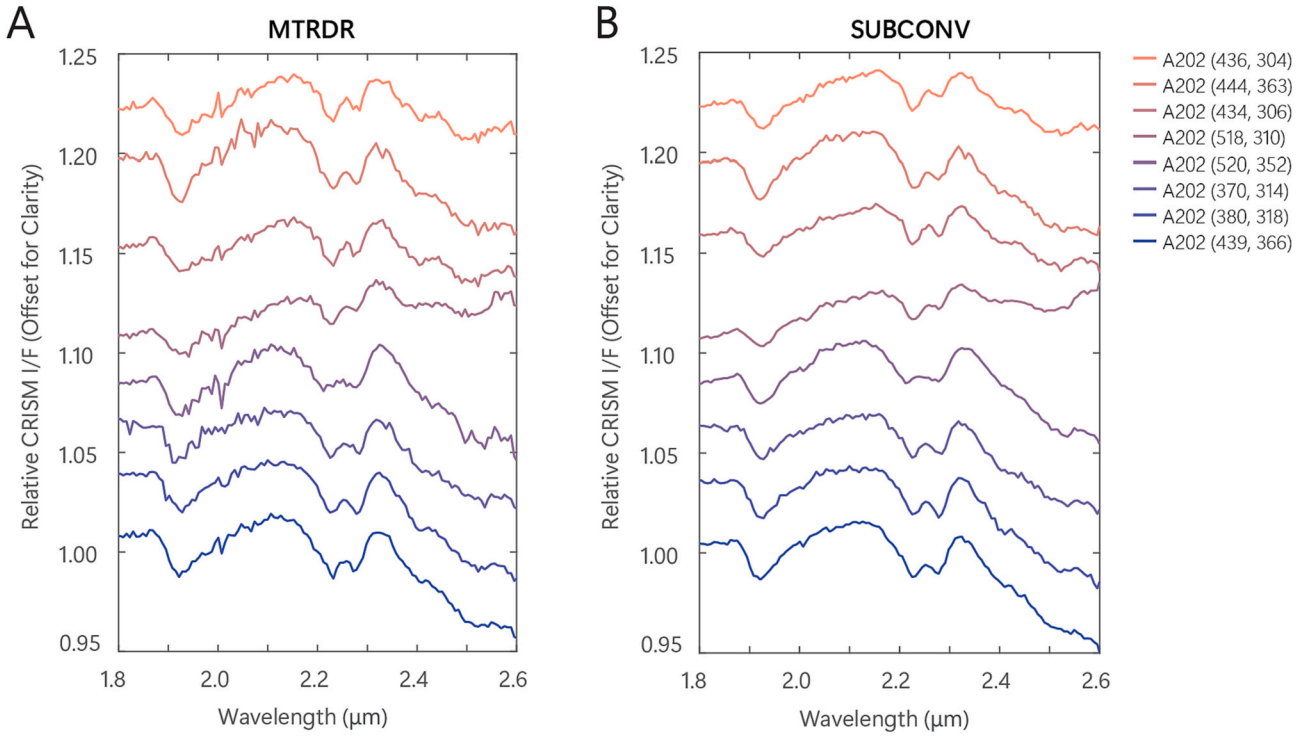

Fig. 2. CRISM spectra from selected spots in image FRT0000A202 illustrating "doublet" shapes from both types of image techniques: (A) MTRDR, (B) SUBCONV.

Table 1
List of the mineral shapes used for the GAN-based mapping.

From the MICA List		Manually Identified
Mg-Olivine	Fe-Olivine	Smectite Mix
Mg-Carbonate	Hydrated Silica	Doublet (Stronger 2.2)
Low Ca-Pyroxene	High Ca-Pyroxene	Doublet (Stronger 2.3)
Kaolinite	Illite	Doublet (Even)
Poly Hyd. Sulfate	Mono Hyd. Sulfate	
Alunite	Jarosite	
Gypsum	Prehnite	
Al-Smectite	Fe/Mg-Smectite	
Hyd. Silica	Hydroxylated Fe-Sulfate	
Serpentine	Epidote	

and 2.6 μm in the feature extraction procedure rather than just one band, ratio, or slope in the spectrum. The manually identified spectral types are listed in Table 1.

Output from the GAN mapping is presented in two forms. The IdentMap image displays each mineral or material detected in the image in a unique color based on the spectral properties over the range 1–2.6 μm. The spectra of these components in the CRISM image are compared to a spectral library of minerals and additional materials measured in the lab, as well as to new classes identified in the image. In the general case, the GAN mapping technique simply compares the GAN space representation of the continuum removed exemplar to that of the representation of the continuum removed test pixel (using cosine distance) and assigns a class label if appropriate. For the three "doublet" classifications where the variations are subtle, an additional fine scale correction is applied to differentiate between the three "doublet" classifications. The fine scale correction is only applied to image pixels detected as members of one of the "doublet" classifications and focuses on the spectral range of 2.1–2.3 μm to accurately map these variants. In order to be classified as identifications and to be included in the IdentMap image, the CRISM spectra must achieve a cosine similarity >0.95 (Saranathan and Parente, 2021) with the shape in the spectral library. However, frequently spectra in CRISM images do not perfectly match the spectral library, but still share many similarities with spectra of the classes under investigation. This could be due to mixing of multiple materials at a pixel level (18 m), poorly crystalline minerals, or other factors. The GuessMap image includes these likely detections that achieve a cosine similarity of 0.85–0.95 (Saranathan and Parente, 2021). The BestGuess image combines the detections made in both the IdentMap and GuessMap into a single image.

The IdentMap and GuessMap images provide visual maps of the suspected classes of minerals and other components. We used these as a guide to check the spectra of individual locations, typically 5 × 5 or 10 × 10 pixels, but sometimes 3 × 3 pixel regions for smaller outcrops. For these analyses we used ENVI software with the CRISM Analysis Tool (CAT) plugin version 7.4 available at the NASA's Planetary Data System (PDS) Geosciences Node: https://pds-geosciences.wustl.edu/missions/mro/crism.htm#Tools.

Once regions were identified in the image containing a spectral doublet between 2.2 and 2.3 μm, we classified these into three groups manually: those having a deeper band closer to 2.2 μm, those having roughly equal band depths, and those having a deeper band closer to 2.3 μm (Fig. 3). CRISM spectra (averaged from several locations to minimize noise) of these three new spectral classes were added to the general set of classes identified with the algorithm for all CRISM images (Saranathan and Parente, 2021). Fig. 4 displays an example of this output, where the BestGuess images include the spectral features of the three newly classified doublet types, as well as other components. The doublet type spectra are the most common components in the two example images.

We initially analyzed both the MTRDR and SUBCONV images for CRISM images FRT0000A202, FRT00009B27, and FRT0000823A (Table 2), where the doublet signatures were strongest to compare the results observed from both techniques. Following the initial confirmation, we expanded the mapping of the doublet materials and associated minerals along the southern wall of the northern canyon using SUBCONV and GAN techniques. The GAN method is optimized for SUBCONV images and cannot be reliably performed for MTRDR datasets. Additionally, there are no established method for mapping such small variations in the doublet absorption features using the MTRDR dataset nor other spectral parameters. As such, we relied on SUBCONV images for our detection and mapping tasks, using the MTRDR images as a spot check to ensure consistency. We subsequently scanned MTRDR images west of the doublet materials in both the southern and northern channel that contained light-toned layered deposits that appeared to have similar morphologies in HiRISE views to the CRISM doublet materials and prepared SUBCONV and identification maps using the GAN technique; we did not, however, find evidence of the spectral doublet feature. Additionally, we analyzed MTRDR image FRT0001751C in the southern channel to characterize the hydrated sulfates located close to a breach in Geryon Montes and we did not observe the presence of the doublet materials.

3. Results

3.1. Spectral "Doublet" alteration product

We screened multiple images across Ius Chasma where light-toned outcrops occur, then selected several CRISM images to investigate in more detail, primarily at the Geryon Montes site, where these unique spectral doublet features occur at the light-toned units. The CRISM

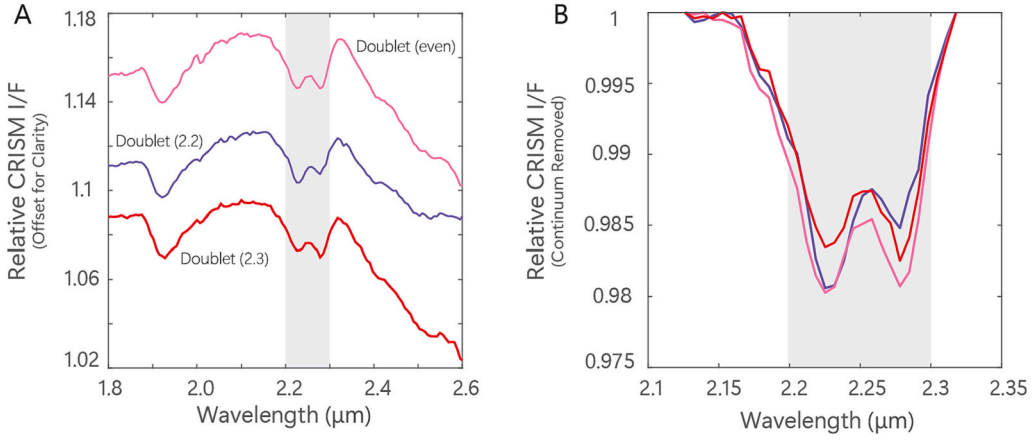

Fig. 3. (A) Exemplar spectra of the three classes of "doublet" material added to the mineral classes for identification. (B) Continuum removed spectra of the three classes of "doublet" material between 2.1 and 2.3 μm.

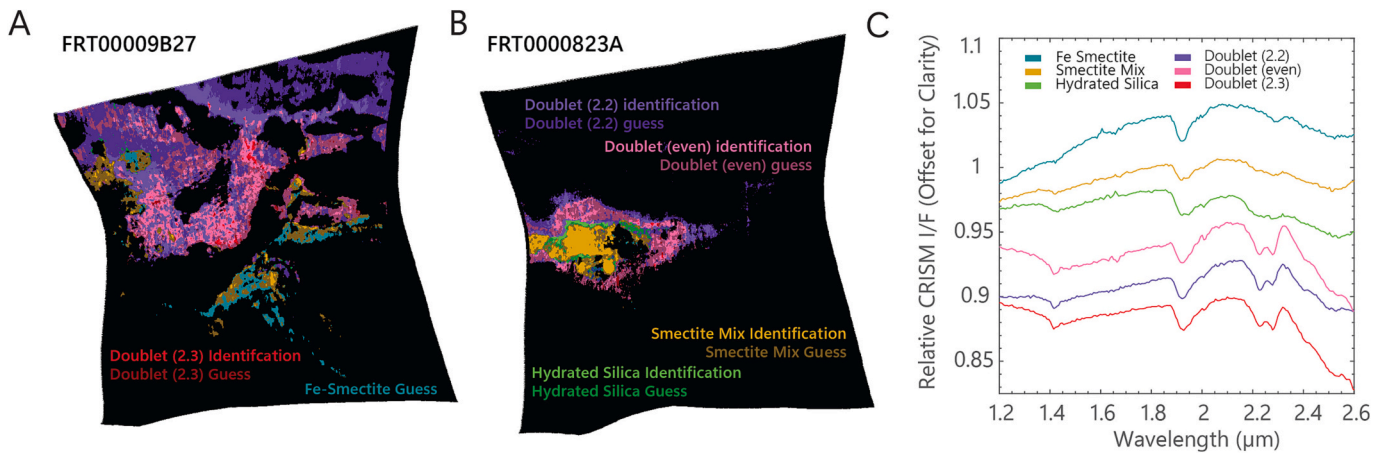

Fig. 4. (A) BestGuess view of the "doublet" and other components in CRISM image FRT00009B27 (B) BestGuess view of the "doublet" and other components in CRISM image FRT0000823A (C) Example spectra of the different mineral identifications from images FRT00009B27 and FRT0000823A.

Table 2
List of CRISM images and the calibration techniques used in this study.

Image	MTRDR	SUBCONV
FRT0000A202	✓	✓
FRT0000A520		✓
FRT00009B27	✓	✓
FRT0000823A	✓	✓
FRT0001712E		✓
FRT00011843		✓
FRT00016626		✓
FRT00009C50		✓
FRT0001135F		✓
FRT0001751C	✓	

CRISM Images Analyzed.

images evaluated in our detailed study are listed in Table 2.

3.1.1. *Doublet characterization*

Fe/Mg smectites, opal, and sulfates have been previously identified in the light-toned deposits within Ius Chasma, in addition to a hydrated mineral phase that was observed with CRISM data, but not well characterized at Ius Chasma (Roach et al., 2010). This hydrated phase, referred to here as the "doublet" material, spans across the 35 km light-toned outcrop in central Ius Chasma, where it is commonly associated with smectites, opal, and mixtures of hydrated components (Fig. 5). The doublet material exhibits absorption features at 1.41 and 1.92 μm due to molecular water, a drop off in reflectance near 2.4 μm, as well as its characteristic spectral doublet feature that occurs between 2.2 and 2.3 μm, with the first absorption band occurring between 2.21 and 2.23 μm and the second absorption band occurring between 2.26 and 2.28 μm. Most commonly, the absorption features occur at 2.225 and 2.278 μm.

We find that the three doublet materials (Fig. 3) exhibit high amounts of variation in the strength of their doublet feature, even when the spectra are averaged over several sites in which the material has been identified (Fig. 6). The band position of these features, however, remains relatively constant. Previous work could not find a similar or corresponding mineral in both the RELAB and USGS spectral libraries (Clark et al., 2007) and it was thought that the closest spectral matches of the doublet material were jarosite, gypsum, or a mixture (Roach et al., 2010). After re-examining the spectral characteristics of the hydrated doublet materials, we considered the identity of the doublet material through the comparison of various laboratory samples that exhibit

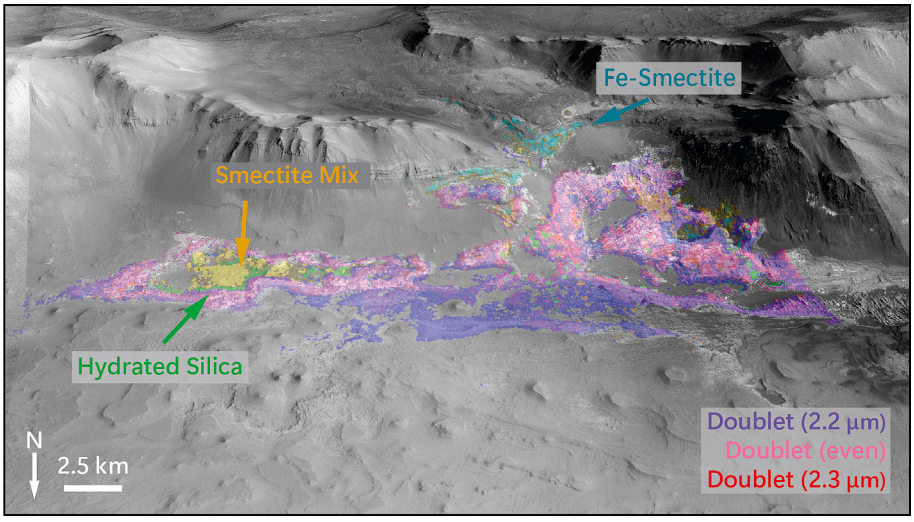

Fig. 5. View of CRISM mineral identification color maps over CTX images on a HRSC DTM. The three doublet occurrences are mapped in pink (doublet material with equal intensity 2.2 and 2.3 μm bands), purple (doublet material with a stronger 2.2 μm band), and red (doublet material with a stronger 2.3 μm band), with smectite occurrences in teal and yellow, and other hydrated silicates mapped in green. (For interpretation of the references to color in this figure legend, the reader is referred to the web version of this article.)

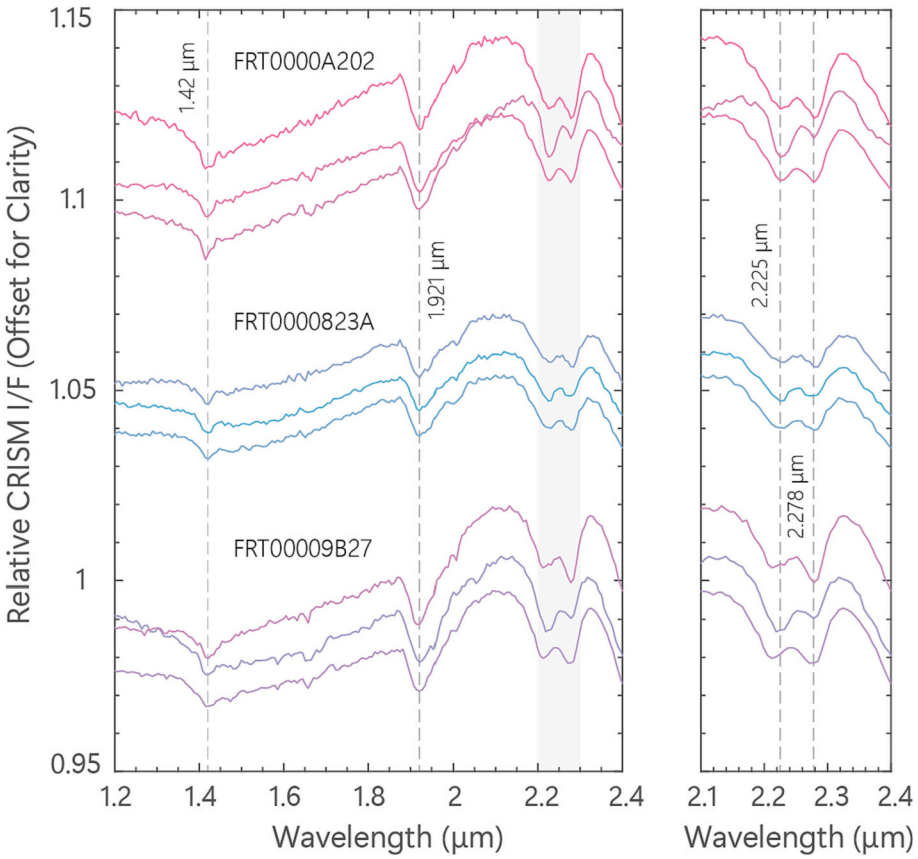

Fig. 6. The average for each doublet type material across three CRISM image locations in Ius Chasma. Notice the variation in band strength between the average doublet types in FRT0000A202, FRT0000823A, and FRT00009B27.

spectral doublet features between 2.2 and 2.3 µm (Fig. 7).

3.1.2. Jarosite and gypsum

Jarosite ($KFe_3^{3+}(OH)_6(SO_4)_2$) exhibits a spectral doublet at 2.21 and 2.26 µm (with the stronger absorption occurring at 2.26 µm) due to Fe-OH vibrations, in addition to narrow absorptions at 1.47 and 1.85 µm due to OH vibrations (Bishop and Murad, 2005; Crowley et al., 2003). Gypsum ($CaSO_4 \bullet 2H_2O$) also exhibits a spectral doublet at 2.21 and 2.26 µm (with the stronger absorption occurring at 2.21 µm), in addition to a distinct triplet absorption between 1.44 and 1.54 µm, as well as absorptions at 1.75 and 1.94 µm, which are due to combinations and overtones of water vibrations and liberations (Bishop et al., 2014; Cloutis et al., 2006).

While both jarosite and gypsum exhibit spectral doublet features between 2.2 and 2.3 µm, their spectral doublet band positions, as well as the relative strength and intensities of these absorption features are not the best match for what is exhibited at Ius Chasma. Additionally, the doublet materials in Ius Chasma do not exhibit the narrow OH related absorptions at 1.47 and 1.85 µm seen in jarosite, nor do they exhibit the distinct gypsum triplet absorptions between 1.44 and 1.54 µm and the water related absorptions at 1.75 and 1.94 µm.

3.1.3. Jarosite / Gypsum mixtures

We considered the possibility that the doublet material may be a mixture of both jarosite and gypsum, with various jarosite/gypsum ratios creating the three distinct types of doublet material. A synthetic 50% jarosite/gypsum mineral mixture produces a spectral doublet characterized by having a weaker ~2.21 µm and a stronger ~2.26 µm absorption feature, in addition to the gypsum triplet between 1.44 and 1.54 µm, and water related absorptions at 1.75 and 1.94 µm (Perrin et al., 2018b). Spectra of natural jarosite/gypsum mixtures collected from the Painted Desert soils in Arizona also exhibits a doublet feature with a stronger ~2.21 µm and a weaker ~2.26 absorption band, in addition to spectral features at 1.41, 1.75, and 1.91 µm (Perrin et al., 2018b). While the spectral doublet feature in both the natural and artificial mixture may be similar to what we are observing at Ius Chasma, the retained spectral character of jarosite and gypsum make it less likely that the mixture of these minerals are producing the doublet materials found at Ius Chasma.

3.1.4. Jarosite / Smectite mixtures

Kaplan et al. (2016) suggested that the doublet material at Ius Chasma may be a jarosite/smectite mixture. We evaluated a series of synthetic jarosite/nontronite mixtures (Usabal et al., 2019) containing 25/75, 50/50, and 75/25 wt% jarosite/nontronite, respectively.

All three laboratory mixtures have spectral features between 1.41 and 1.47 µm, in addition to a feature at 1.85 µm in the 75/25 mixture due to OH overtones and combination bands in jarosite, and a water related feature at 1.91 µm. The 50/50 and 25/75 jarosite/nontronite mixtures produce a spectral doublet feature at ~2.21 and ~ 2.27 µm, in addition to a weak 2.29 µm feature. The 75/25 jarosite/nontronite mixture does not produce a spectral doublet feature, however it does contain a strong 2.29 µm feature due to OH combination bands in nontronite (Bishop et al., 2020). While the spectral doublet features in the jarosite/nontronite mixtures may be spectrally similar to what is observed at Ius Chasma, the absence of jarosite (1.47 and 1.85 µm) and nontronite (2.29 µm) related features in the doublet materials makes it unlikely that the doublet materials are simply physical mixtures of the minerals jarosite and nontronite.

3.1.5. Acid altered clays

Given the association between smectites and the doublet material in

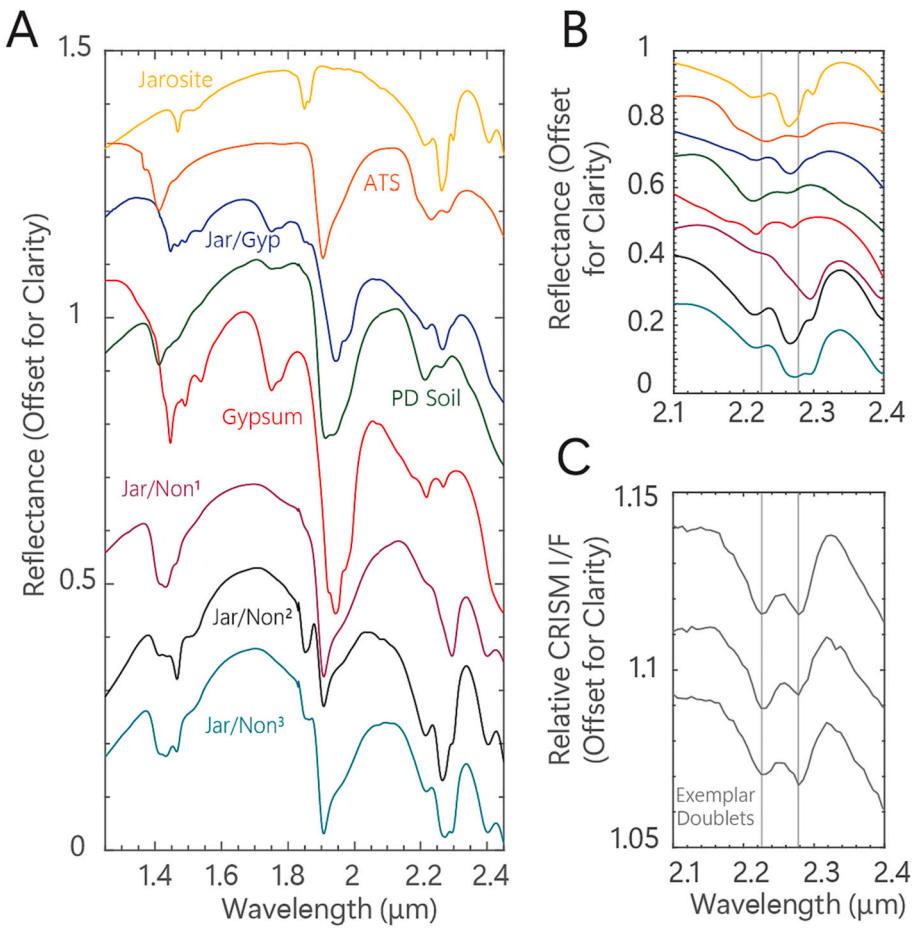

Fig. 7. (A) Reflectance spectra of minerals and mineral mixtures that exhibit a spectral doublet feature between 2.2 and 2.3 μm and were considered in this study: Jarosite (Bishop and Murad, 2005), ATS altered for 2 h (Madejová et al., 2009), a 50/50 wt% jarosite/gypsum mineral mixture (Jar/Gyp) prepared in the lab (Perrin et al., 2018b), gypsum (Bishop et al., 2014), a 25/75, 75/25, and 50/50 jarosite/nontronite mineral mixture Jar/Non1, Jar/Non2, Jar/Non3 respectively (Usabal et al., 2019), an orange soil sample from the Painted Desert (PD soil), which includes ~69 wt% jarosite, ~14 wt% quartz, ~10 wt% gypsum, and ~ 7 wt% montmorillonite (Perrin et al., 2018a). (B) Zoomed in view of the spectral doublet features in laboratory minerals and mixtures. (C) Exemplar spectra of the three doublet type materials found at Ius Chasma.

Ius Chasma, we considered the possibility that the doublet material may be an alteration product of the smectites found across the region. We analyzed spectra of an acid treated ferruginous smectite, Swa-1, measured by Madejová et al. (2009). Several phyllosilicate samples were treated with HCl to determine the influence of acid alteration on their spectral properties (Madejová et al., 1990, 2007, 2009). These acid treated smectite (ATS) samples have a spectral doublet feature at ~2.23 and ~ 2.28 μm, in addition to absorption features at 1.41 and 1.91 μm due to the presence of molecular water in the sample, and a drop off in reflectance near 2.4 μm (Fig. 8). The spectral similarities of not only the spectral doublet feature, but also other absorption features, found in both the ATS and doublet materials at Ius Chasma, suggests that the doublet material may be an acid altered smectite mineral. Variations in the relative strengths of the doublet bands were also observed due to changes in the length of acid treatment (Madejová et al., 1990, 2007, 2009), where a stronger band was observed near 2.23 μm for a longer exposure to acidic conditions. We favor formation of the doublet materials at Ius Chasma through acid alteration of the smectites, with the doublet variation attributed to differences in the solution chemistry, water/rock ratio, substrate, or duration of the alteration process.

3.2. *Properties of materials and geomorphology of the Geryon Montes region of Ius Chasma*

Ius Chasma is connected to Noctis Labyrinthus in the west and to Melas Chasma in the east, stretching nearly 850 km in length and 120 km in width. Within Ius Chasma are tributary canyons, with the longest most prominent tributary canyon containing the light-toned deposits. The surface of the light-toned deposits at Ius Chasma are characterized by their polygonal fractures which could have formed through the desiccation of hydrated materials or thermal contraction. These light-toned deposits are described in depth by (Roach et al., 2010).

The mountains that make up Geryon Montes separate Ius Chasma into southern and northern canyons, reaching heights upwards of 5 km and local widths of up to 26 km (Dębniak et al., 2017). The northern canyon of Ius Chasma contains smectites and other hydrated silicates, whereas the southern canyon contains both MHS and PHS (Fig. 9) and shows no evidence of containing doublet like materials. These sulfates likely evaporated from a concentrated parent brine that pooled within the southern canyon (Roach et al., 2010), with the brine initially precipitating out PHS followed by MHS near the end stages of evaporation (Spencer, 2000). The sulfates observed at Ius Chasma on the south side of Geryon Montes are similar to the MHS and PHS observed in other chasmata and likely needed long-term warm waters (Al-Samir et al., 2017). The smectite-bearing units and hydrated silica found in the northern canyon are typical of these materials observed elsewhere on Mars in the ancient Noachian rocks (e.g Mustard et al., 2008). The most prominent aqueous outcrop after the doublet units is the smectite mixture mapped in gold that contains some spectral features of Fe/Mg-smectite with a weaker band near 2.3 μm. Occasional occurrences of Fe-

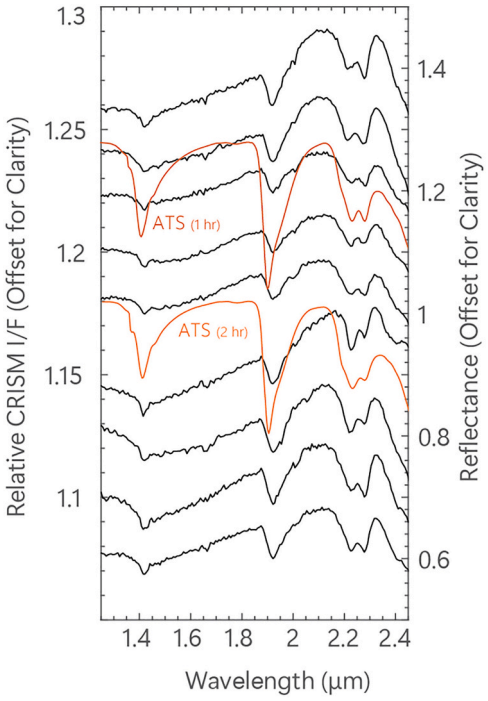

Fig. 8. Spectra of several Ius Chasma doublet sites compared to two acid treated smectite (ATS) samples altered for one and two hours (see Madejová et al., 2009) in orange. The ATS samples display the most spectral similarities to the doublet materials, as they display similar water band positions at ~1.41 and ~ 1.91 μm, in addition to strikingly similar doublet features at ~2.23 and ~ 2.28 μm, as well as a drop off in reflectance at ~2.4 μm.

rich smectite with a band near 2.29 μm are mapped in teal and are generally observed in outcrops not bordering the smectite mixture materials. The hydrated silica unit (green) is more common than the Fe-rich smectite and typically does border the smectite mixture unit. Example spectra of these units are shown in Fig. 4.

Mineral identification maps are presented in Figs. 5, 10a, and 11. Smectite mixture occurrences are mapped in yellow, iron smectites are mapped in teal, hydrated silica is mapped in green, with the doublet occurrences mapped in pink (doublet characterized by having equal intensity 2.2 and 2.3 μm bands), purple (doublet characterized by having a stronger 2.2 μm band), and red (doublet characterized by having a stronger 2.3 μm band). The morphologies of the doublet materials located in the northern canyon are shown in Fig. 10a. The pink and purple units mapped with CRISM correspond to fractured and brecciated light-toned materials. Smooth ridges can be present with a general N-S orientation, consistent with erosion by downslope and upslope winds along the steep walls of the canyon. Brightness variations are common but do not correspond to specific layers or elevations. Some irregular patches within the pink and purple doublet units are much brighter than the adjacent materials indicating compositional and/or physical heterogeneities in these deposits. The most prominent difference in morphology between the pink and purple colors appears to be due to the presence of darker loose sediments on the surface of the purple unit (Fig. 10c) that is not seen on the pink unit (Fig. 10b). Note that these "darker" loose sediments are darker than the pink unit, but still brighter than the surrounding materials. Coverage of the red doublet (stronger 2.28 μm band) is limited in HiRISE image ESP_048136_1725 and thus it is difficult to determine differences in morphology of the red unit compared to the pink and purple units.

One possible explanation for the relationship between the pink and purple units is that the darker loose sediments contain a band near 2.2 μm but not near 2.3 μm and that they partially cover the pink unit, resulting in a stronger intensity of the 2.23 μm band of the doublet when

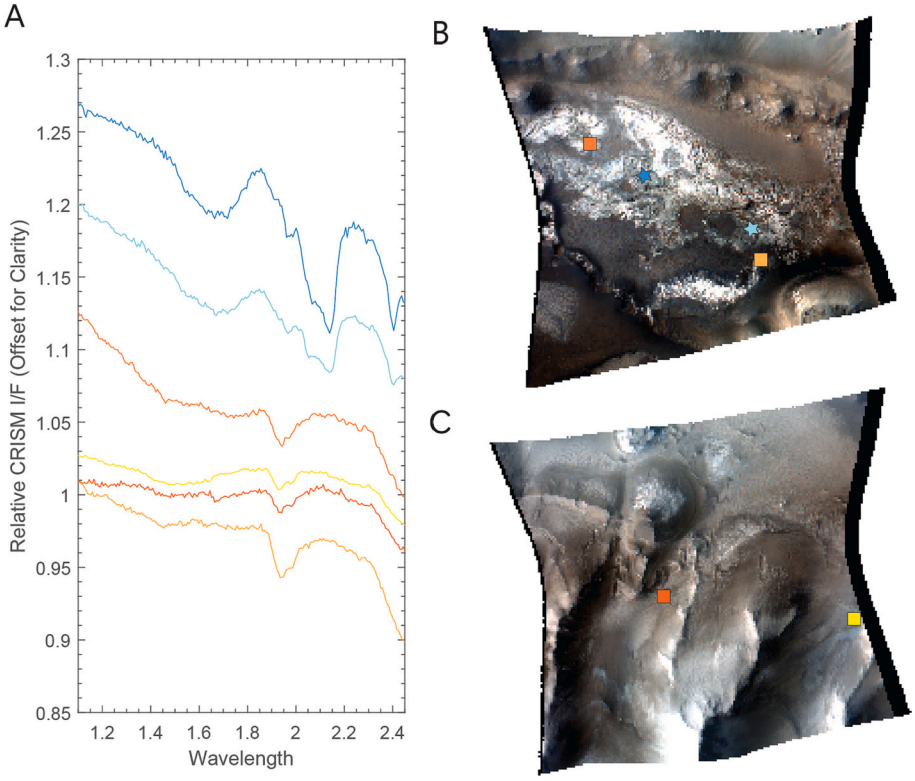

Fig. 9. (A) Spectra of the monohydrated sulfates (MHS) and polyhydrated sulfates (PHS) in the southern canyon (B) Views of the southern canyon of Ius Chasma in CRISM images FRT00016626 and (C) FRT00011843. Locations marked with squares correspond to the PHS and locations marked with stars correspond to the MHS shown in (A).

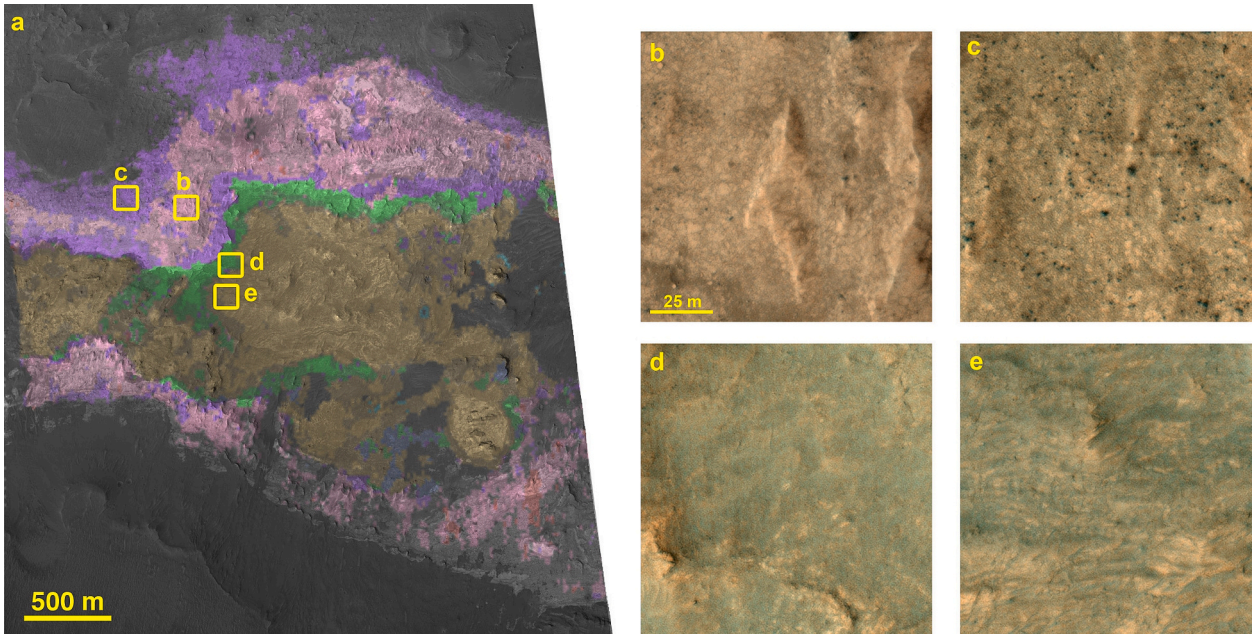

Fig. 10. (a) HiRISE RED image ESP_048136_1725 with spectral units from CRISM image FRT0000823A mapped using the same color scheme in Fig. 5. The three doublet occurrences are mapped in pink (doublet material with equal intensity 2.2 and 2.3 μm bands), purple (doublet material with a stronger 2.2 μm band), and red (doublet material with a stronger 2.3 μm band), with smectite occurrences in yellow and other hydrated silicates mapped in green. Yellow squares identify blowups in b-e. (b-e) Blowups taken from HiRISE ESP_048136_1725 RGB image showing the morphologies corresponding to the different colors. Scale bar in (b) is the same for (c-e). (For interpretation of the references to color in this figure legend, the reader is referred to the web version of this article.)

viewed by CRISM at 18 m spatial resolution. This could be possible if the loose sediment contains opal. Spectral mixing of the broad hydrated silica-type band near 2.1 μm with the narrower 2.23 μm band observed for the doublet outcrops could result in a stronger band at 2.23 μm compared to 2.28 μm with only a minor shift in band position near 2.23 μm. Another interpretation is that the darker loose sediments are sourced from a more strongly altered material where the 2.23 μm band is stronger compared to the 2.28 μm band. Potentially, the more altered unit is less cohesive and eroded faster through wind erosion, becoming a mobile sediment unit. In this scenario the pink materials would have experienced more acidic alteration than the red materials and the purple unit would have experienced the most acidic alteration but is no longer a coherent material, but rather mobile and partially covering the pink unit. This would explain variations in the intensities of the doublet bands.

In the case of the green (hydrated silica) and gold (Fe/Mg-smectite mixture) units, both appear to have a surficial veneer of darker materials making them lower in brightness relative to the pink and purple units. Meter-scale layering is present throughout much of the gold unit, as are aeolian ripples. The smooth N-S ridges commonly seen in the pink and purple units are not observed in the gold unit. Instead, rough blocky ridges and knobs shedding large boulders are seen only in the gold unit.

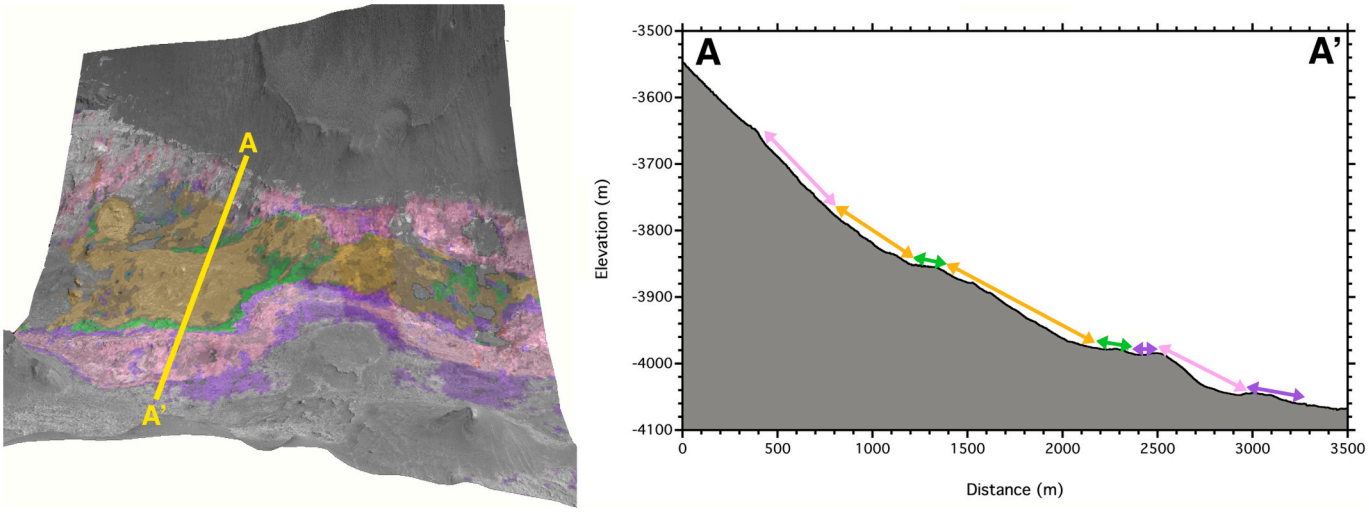

Fig. 11. (left) HiRISE DTM perspective view at 3× V.E. with the same color scheme for the CRISM mineral map in Figs. 5 and 10 overlain. The three doublet occurrences are mapped in pink (doublet material with equal intensity 2.2 and 2.3 μm bands), purple (doublet material with a stronger 2.2 μm band), and red (doublet material with a stronger 2.3 μm band), with smectite occurrences in yellow and other hydrated silicates mapped in green. The location where the topographic profile was taken is shown by the yellow line. (right) Topographic profile showing the locations of each spectral color by the arrows with the same colors. Note how the units drape along the lower wall rock slopes and do not correspond to a particular elevation.

The difference in morphology between the green and gold units is not well constrained from the HiRISE images. Thus, there appear to be primarily two distinct units based upon morphology, with the pink and purple colors representing one unit (with the thicker dark surficial mantle occurring on the purple colored regions) and the gold and green colored materials representing a different unit.

The stratigraphy for the different colors does not correlate to elevation as shown by the DTM perspective view and topographic profile shown in Fig. 11. All the units are draped along the lower wall rock slopes of northern Geryon Montes between elevations ~ − 3600 m to −4100 m. Both the green and purple colored regions correspond to shallower slopes relative to the pink and gold colored regions. Because loose debris is more favorable to collect on shallower surfaces, the purple and green areas are more likely to have more dark debris on their surfaces that in turn would affect the CRISM spectra relative to the pink and gold regions.

Topography derived from MOLA data has also been useful for understanding why the doublet materials could have formed here. The section of Geryon Montes mountains that collocates with the doublet material in Ius Chasma has a significantly lower ridge height than ridge localities to both the east and west of the observed doublet unit (Fig. 12). It is likely that pooling water forming the parent brine in the southern sulfate-rich canyon overflowed at the breach in Geryon Montes where the topography shows the lowest height over the ridge formation into the northern canyon where the doublet materials are observed. The morphology and topology observed along the upper deposit exhibits rounded edges, heterogeneity, and topography variations (Fig. 13) that are consistent with fluid flow in this region and therefore supportive of an inflow of brine from the southern canyon. The jumbled, blocky morphology observed here at Ius Chasma is similar to the blocky deposits identified along the wall rock and floor to the east in Melas Chasma. The Melas deposits have been interpreted as evidence for soft sediment deformation by slumping and/or sliding of sulfates and clay mixtures down the wall rock slopes (Metz et al., 2010; Weitz et al.,

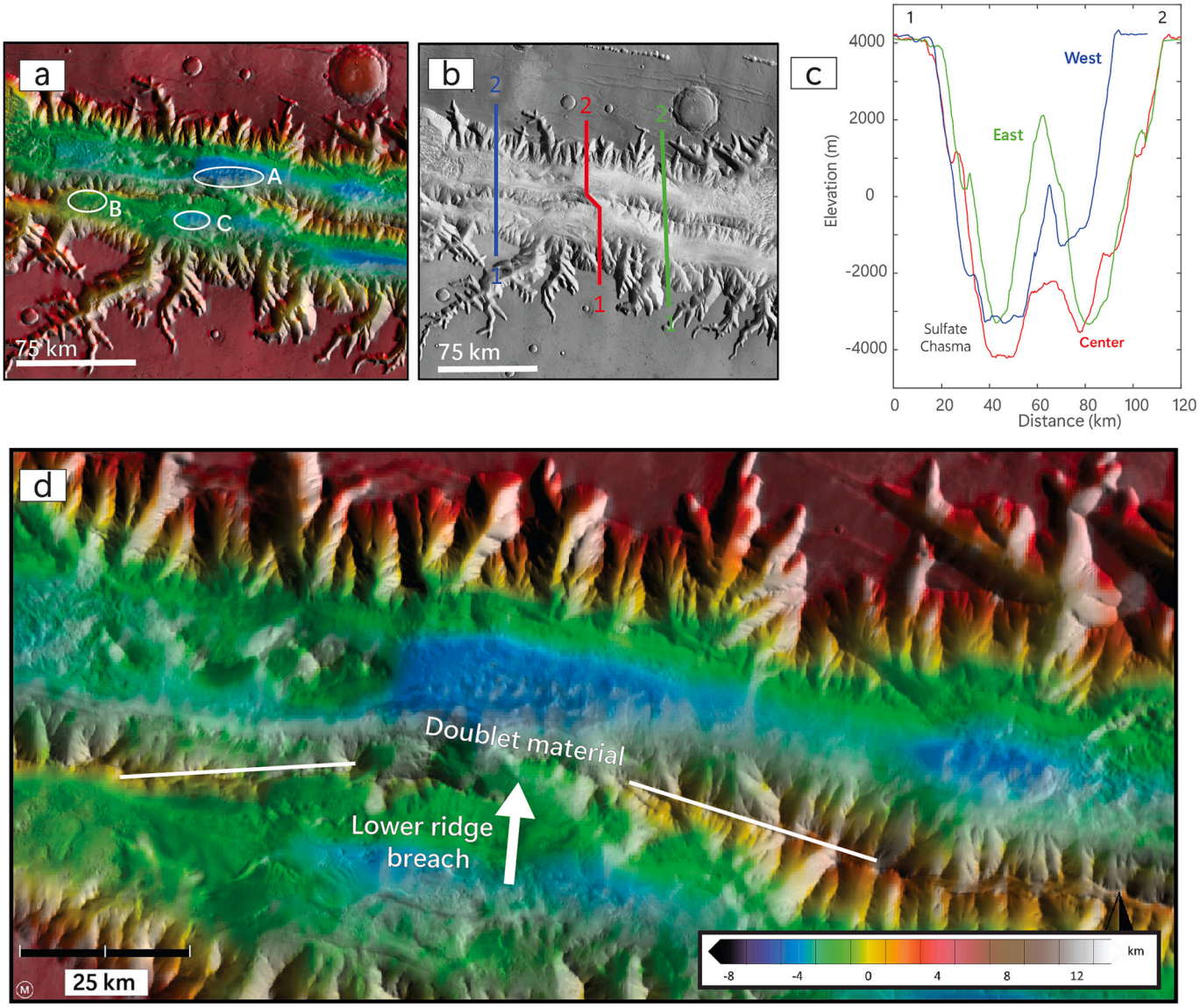

Fig. 12. (A) Views of Ius Chasma indicating the locations of doublet materials (a) and two sites containing sulfates (b,c). (B) THEMIS daytime image with three profile line marked. (C) Profile from N to S across Geryon Montes and the sulfate-bearing side of the chasma for the western, central, and eastern profiles. Note the low elevation of the Geryon Montes mountains associated with the center profile (red) and the low elevation of the northern canyon floor where the doublet materials were found. (D) MOLA topography with lower depths shown in blue. The white lines show the top of the Geryon Montes mountains, and the white arrow identifies the lowest elevation along the mountains where there appears to be a breach from the south to the northern canyon. (For interpretation of the references to color in this figure legend, the reader is referred to the web version of this article.)

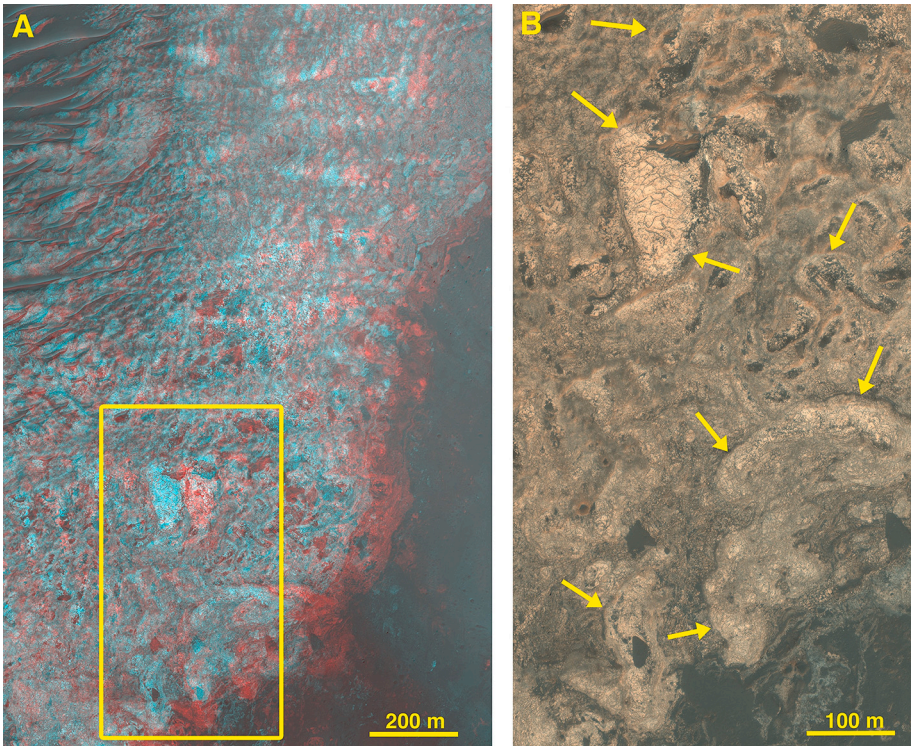

Fig. 13. Example of the jumbled, deformed morphology of the Ius deposit at the location of the wall rock breach in Geryon Montes. (A) HiRISE anaglyph showing the uneven topography across the deposit, with a higher standing heterogeneous darker matrix above rounded, brighter materials. HiRISE stereo images ESP_060136_1725 and PSP_007074_1725 were used to produce this anaglyph. Yellow rectangle identifies the blowup shown in (B). (B) Rounded edges identified by yellow arrows do not always follow the slope along the wall rock (from lower right to upper left) and are variable in topography, consistent with flow of the doublet unit downhill rather than intact bedrock exposed within the wall rock. Portion of HiRISE enhanced RGB image ESP_060136_1725. (For interpretation of the references to color in this figure legend, the reader is referred to the web version of this article.)

2015), consistent with our proposed flow origin for the Ius Chasma deposit.

As the brine overflowed from the southern to northern canyons at this gap in Geryon Montes, the brine likely flowed down the wall rock following the slope of the canyon and penetrated into the rock. If substantial flows had occurred, the largest alteration outcrops would have occurred along the floor of the northern canyon. Because we observe the greatest abundance of alteration phases exposed along the lower slopes of the wall rock, the brine flows appear to have been concentrated in these regions, rather than on the floor of the north channel. We propose that these sulfate-rich brines altered the phyllosilicates in or on the wall rock to form the doublet materials. The transect in Fig. 11 shows that the doublet materials are present above and below the phyllosilicates and hydrated silica. This may indicate that these ancient smectites were altered by the brine both along the exposed surfaces, as well as along the borders of the smectite units if brine was able to seep through the regolith and more aggressively alter these smectite outcrops along the edges. Thus, thinner regions of smectite along the edges of the outcrop could be nearly completely altered, while the thicker smectite-bearing regions near the center of the outcrop are still partially intact in the wall rock. These thicker regions likely contained a veneer of brine-altered material on their surface initially that was then scoured off over time. In contrast, the regions where the doublet materials are observed today could have initially been thinner smectite deposits that became doublet units during alteration and are still observed today, although the original surface of the doublet material was likely scoured off over time. Alternatively, given that the doublet unit is observed both to the west at Noctis Labyrinthus and to the east in Melas Chasma, the unit may have originally been deposited as a volcanic ash unit (containing smectites) across the region and then subsequently altered as described above by the brine overflowed at this gap.

4. Potential geochemical formation processes

4.1. Overflow from south canyon

Phyllosilicates are observed together with sulfates throughout much of the region from Noctis Labyrinthus to Ius Chasma and Melas Chasma and may have resulted from aqueous alteration of pyroclastic ash deposits (Weitz et al., 2010). Fe/Mg-smectites are observed throughout the southern highlands of Mars and are thought to have formed through aqueous alteration of basalt during the Noachian (e.g. Murchie et al., 2009a; Bishop et al., 2019). Spectral doublet units occur in a few localities on Mars including Noctis Labyrinthus (Weitz et al., 2011) and Mawrth Vallis (Bishop et al., 2020), with the largest outcrop observed at Ius Chasma on the north side of Geryon Montes. Smectites alter in acidic solutions to form a spectral doublet feature (Madejová et al., 2009), which is likely what occurred at Geryon Montes. We posit that this doublet material formed by brine overflowing from the MHS/PHS pool on the south of Geryon Montes to form a brine-sludge on the south wall of the northern canyon along Geryon Montes as the brine interacted with fine-grained particles, including phyllosilicates. Brine viscosity increases with sulfate and chloride content as well as with the presence of insoluble fines and lower temperatures (e.g., Chevrier et al., 2009; Sánchez-Juny et al., 2019). If the brine had been a liquid-like low viscosity consistency, it would have flowed to the floor of the canyon and altered the materials there. Instead, we observed the strongest outcrops of the doublet material along the south wall slopes of this northern canyon which suggests a higher viscosity for the brine-sludge. Another possibility is that neutral or dilute waters along the floor of the northern channel served to dilute the brine concentration at lower elevations. This scenario is less likely though because if a standing brine was present in the north channel, we would expect to see evidence of alteration

Fig. 14. Proposed formation sequence of the doublet materials at Ius Chasma: (1) Ancient smectite outcrops, either exposed within the wall rock as bedrock or super imposed on it as volcanic ash, along the southern wall of the northern Geryon Montes canyon in Ius Chasma. (2) Sulfate brines pooled in the southern canyon where sulfates formed, then overflowed into the northern canyon, seeping down the canyon wall, but not extending to the canyon floor. (3) Interaction with the brine solution would have altered the smectites to form the doublet material, with changes in the solution chemistry, water/rock ratio, or time of alteration creating the differences in doublet material.

minerals along the floor and these are not observed. Other regions of the wall containing hydrated silica may have formed from brine alteration of basaltic ash where smectites were not present in the ancient canyon walls. A similar process could have occurred at neighboring canyons where doublets are also observed. Because the doublet materials at Ius Chasma have the strongest spectral features relative to other locations, they appear to be the most concentrated occurrence of this unique alteration phase. The proposed formation sequence is illustrated in Fig. 14.

4.2. Comparison with terrestrial analog sites

Terrestrial analog sites featuring phyllosilicate-sulfate assemblages provide insights into potential geochemical environments governing formation of this doublet spectral feature. The Ius Chasma outcrop at Geryon Montes is consistent with alteration of pre-exisiting Fe/Mg-smectite to form large outcrops of three types of spectral doublet units along with minor occurrences of Al-phyllosilicates and hydrated silica. This transition from Fe-rich smectite to sulfate/silica/Al-phyllosilicate assemblages can provide evidence about the geochemical history of the region including changes in pH, salt levels, and/or water/rock ratio.

Evaporite environments supporting salars or shallow salt ponds in the Antofagasta region of Chile, north of the Atacama desert include assemblages of gypsum, halite, hydrated silica, and phyllosilicates (Flahaut et al., 2017). Many of the gypsum-bearing rocks and sediments from that study exhibit spectral doublet features, although they are weaker than those observed at Ius Chasma. Similar rocks and sediments have been observed in salt ponds of the Yilgarn Craton of Western Australia, where mixtures of phyllosilicates, opal, gypsum, alunite, and jarosite have been investigated (Benison and Bowen, 2006; Bowen et al., 2013; Story et al., 2010). Based on these analog sites, evaporites alone would not be good analogs for the Ius Chasma site, but brines similar to some of these evaporite sites could have altered the ancient smectites at Ius Chasma to form the observed doublets.

Solfataric alteration of volcanic ash at Kilauea, HI (Bishop et al., 2005) and LaSolfatara, Italy (Flahaut et al., 2019) has produced mixtures of nontronite, jarosite, gypsum, and opal. While this scenario is unlikely to explain the doublet unit observed at Ius Chasma, this scenario may provide a viable explanation for the doublet units observed at other regions on Mars.

The extensive doublet units observed at Ius Chasma are attributed to a more regional process and could be due to alteration of the ancient Fe/Mg-smectite present in Noachian basalt or volcanic ash in a muddy sludge-type setting as the brine interacts with the phyllosilicates and associated fine-grained materials of this region. The presence of different types of doublet units here is consistent with changes over time in the pH, salt levels, or water/rock ratio, or simply with the degree of alteration of the smectite in the acidic sludge. Madejová et al. (2009) documented changes in the intensity of the spectral doublet feature in smectites with progressive acidic alteration in the laboratory. This is most consistent with the changes in relative abundance of the doublet bands in our study.

4.3. Summary

Previous work (Kaplan et al., 2016; Roach et al., 2010) investigated the enigmatic materials found in the light-toned deposits at Ius Chasma, although the identity of the double materials remained unresolved at that time. Here we re-examined the potential composition of the doublet material with improved image calibrations and detailed mapping of the doublet occurrences. These significantly improved spectral images allowed for documentation of variations among the doublet-type units, and three types of doublet units were identified and mapped along the wall of the northern canyon of Ius Chasma near the breach in the Geryon Montes. The spectra of the Ius Chasma doublets exhibit water bands near 1.4 and 1.9 μm, similar to smectite clays, as well as a pair of narrow bands near 2.23 and 2.27 μm that vary in relative intensity. The relative intensities of these doublet bands were used to define three units: where both bands have similar band strengths, where the ~2.23 μm band is stronger, and where the ~2.27 μm band is stronger.

Three possible compositions of the doublet material at Ius Chasma were investigated:

1) Jarosite / gypsum mixture
2) Jarosite / smectite mixture
3) Acid altered smectite

None of these potential compositions and formation mechanisms provides a perfect fit for the spectral properties of the doublet materials in our study. However, of these possibilities, we favor the acid alteration scenario whereby the doublet material at Ius Chasma forms where acidic brines altered pre-existing smectites in or on the wall rock. Variations in the doublet material may be attributed to compositional changes in the underlying substrate, changes to the solution chemistry in the pooling waters over time, or simply duration of the brine and hence extent of alteration.

Correlation of the mineral maps from CRISM with the higher spatial resolution of HiRISE enabled comparison of the morphologies of the different alteration units at meter scale. These results indicated similarities in the smectite-mixture unit and the hydrated silica unit as well as similarities among the doublet units. These observations are consistent with a common origin for the different doublet units. Mapping transects of these components along the wall rock using CRISM results overlain on a HiRISE DTM shows shallower slopes where the hydrated silica and purple-colored doublet units are present. This may indicate collection of more dust and mobile components at these locations.

Correlation of the mineral maps from CRISM with the HRSC stereo views provides geologic context across several CRISM images and documents formation of the doublet units surrounding the smectite in some cases, likely where a thicker smectite unit existed prior to brine deposition. Other regions of the aqueous outcrops are dominated by the doublet materials, leaving few remnants of the smectite visible at the surface. This could have occurred where the original smectite units were thinner and more readily altered by the acidic brine and/or where thicker acid altered smectite units were produced. The stratigraphy and locations of the alteration materials in the CRISM over HRSC view (Fig. 5) also shows that the largest smectite outcrop occurs further from

the breach in the Geryon Montes and that most of the altered materials directly below the breach are completely altered to the doublet units described in our study. Further, the purple-colored doublet unit that contains a stronger 2.23 μm band and is consistent with increased acid alteration, occurs downslope from the less altered doublet outcrops. This supports our brine alteration model in that the lower elevation, shallower sloped horizon below the breach at Geryon Montes exhibits the strongest alteration.

Declaration of Competing Interest

The authors declare that they have no known competing financial interests or personal relationships that could have appeared to influence the work reported in this paper.

Data availability

Data will be made available on request.

Acknowledgements

We greatly appreciate the efforts of the CRISM, HiRISE, and HRSC teams for collecting and archiving the images used in this study. We are grateful to support from the NASA Astrobiology Institute (grant #NNX15BB01) to JLB, NASA's Mars Data Analysis Program (grant #NNX19K1230) to JLB, CMW, and KW, and NASA's Planetary Data Archiving, Restoration, and Tools Program (grant #NNX16AG48G) to MP, YI, and AMS for this work. We are also thankful for suggestions from L. Roach, S. Murchie, and E. Rampe that improved this paper.

References

Al-Samir, M., Nabhan, S., Fritz, J., Winkler, A., Bishop, J.L., Gross, C., Jaumann, R., 2017. The paleolacustrine evolution of Juventae Chasma and Maja Valles and its implications for the formation of interior layered deposits on Mars. Icarus 292, 125–143. https://doi.org/10.1016/j.icarus.2016.12.023.

Benison, K., Bowen, B., 2006. Acid saline lake systems give clues about past environments and the search for life on Mars. Icarus 183, 225–229. https://doi.org/10.1016/j.icarus.2006.02.018.

Bibring, J.-P., Langevin, Y., Mustard, J.F., Poulet, F., Arvidson, Raymond, Gendrin, A., Gondet, B., Mangold, N., Pinet, P., Forget, F., Berthé, M., Bibring, J.-P., Gendrin, A., Gomez, C., Gondet, B., Jouglet, D., Poulet, F., Soufflot, A., Vincendon, M., Combes, M., Drossart, P., Encrenaz, T., Fouchet, T., Merchiorri, R., Belluci, G., Altieri, F., Formisano, V., Capaccioni, F., Cerroni, P., Coradini, A., Fonti, S., Korablev, O., Kottsov, V., Ignatiev, N., Moroz, V., Titov, D., Zasova, L., Loiseau, D., Mangold, N., Pinet, Patrick, Douté, S., Schmitt, B., Sotin, C., Hauber, E., Hoffmann, H., Jaumann, R., Keller, U., Arvidson, Ray, Mustard, J.F., Duxbury, T., Forget, François, Neukum, G., 2006. Global mineralogical and aqueous Mars history derived from OMEGA/Mars express data. Science 312, 400–404. https://doi.org/10.1126/science.1122659.

Bishop, J.L., Murad, E., 2005. The visible and infrared spectral properties of jarosite and alunite. Am. Mineral. 90, 1100–1107. https://doi.org/10.2138/am.2005.1700.

Bishop, J.L., Schiffman, P., Lane, M.D., Dyar, M.D., Southard, R.J., 2005. Solfataric alteration in Hawaii as a mechanism for formation of the sulfates observed on Mars by OMEGA and the MER instruments. In: Presented at the Lunar Planet. Sci. XXXVI, Houston, TX.

Bishop, J.L., Parente, M., Weitz, C.M., Noe Dobrea, E.Z., Roach, L.H., Murchie, S.L., McGuire, P.C., McKeown, N.K., Rossi, C.M., Brown, A.J., Calvin, W.M., Milliken, R., Mustard, J.F., 2009. Mineralogy of Juventae Chasma: Sulfates in the light-toned mounds, mafic minerals in the bedrock, and hydrated silica and hydroxylated ferric sulfate on the plateau. J. Geophys. Res. 114 https://doi.org/10.1029/2009JE003352. E00D09.

Bishop, J.L., Lane, M.D., Dyar, M.D., King, S.J., Brown, A.J., Swayze, G.A., 2014. Spectral properties of ca-sulfates: gypsum, bassanite, and anhydrite. Am. Mineral. 99, 2105–2115. https://doi.org/10.2138/am-2014-4756.

Bishop, J.L., Schiffman, P., Lane, M.D., Southard, R.J., Gruendler, L., 2015. Solfataric alteration at Hawaii as a potential Analog for Martian surface processes. In: Presented at the AGU Fall Meeting, San Francisco, CA.

Bishop, J.L., Flahaut, J., Perrin, S.L., 2019. Characterizing environments containing complex phyllosilicate-sulfate assemblages as analogs for Mars. In: Presented at the EPSC-DPS Joint Meeting, Geneva, Switzerland.

Bishop, J.L., Gross, C., Danielsen, J., Parente, M., Murchie, S.L., Horgan, B., Wray, J.J., Viviano, C., Seelos, F.P., 2020. Multiple mineral horizons in layered outcrops at Mawrth Vallis, Mars, signify changing geochemical environments on early Mars. Icarus 341, 113634. https://doi.org/10.1016/j.icarus.2020.113634.

Bowen, B.B., Story, S., Oboh-Ikuenobe, F., Benison, K.C., 2013. Differences in regolith weathering history at an acid and neutral saline lake on the Archean Yilgarn craton and implications for acid brine evolution. Chem. Geol. 356, 126–140. https://doi.org/10.1016/j.chemgeo.2013.08.005.

Carr, M.H., Head, J.W., 2010. Geologic history of Mars. Earth Planet. Sci. Lett. 294, 185–203. https://doi.org/10.1016/j.epsl.2009.06.042.

Chevrier, V.F., Ulrich, R., Altheide, T.S., 2009. Viscosity of liquid ferric sulfate solutions and application to the formation of gullies on Mars. J. Geophys. Res. 114, E06001 https://doi.org/10.1029/2009JE003376.

Chojnacki, M., Hynek, B.M., 2008. Geological context of water-altered minerals in Valles Marineris, Mars. J. Geophys. Res. 113, E12005 https://doi.org/10.1029/2007JE003070.

Clark, R., Swayze, G., Wise, R., Livo, K.E., Hoefen, T.M., Kokaly, R.F., Sutley, S.J., 2007. Data USGS Digital Spectral Library splib06a (Data Series 231), Data Series.

Cloutis, E., Hawthorne, F., Mertzman, S., Krenn, K., Craig, M., Marcino, D., Methot, M., Strong, J., Mustard, J., Blaney, D., 2006. Detection and discrimination of sulfate minerals using reflectance spectroscopy. Icarus 184, 121–157. https://doi.org/10.1016/j.icarus.2006.04.003.

Crowley, J.K., Williams, D.E., Hammarstrom, J.M., Piatak, N., Chou, I.-M., Mars, J.C., 2003. Spectral reflectance properties (0.4–2.5 μm) of secondary Fe-oxide, Fe-hydroxide, and Fe-sulphate-hydrate minerals associated with sulphide-bearing mine wastes. Geochem.: Explor., Environ., Anal. 3, 219–228. https://doi.org/10.1144/1467-7873/03-001.

Dębniak, K., Mège, D., Gurgurewicz, J., 2017. Geomorphology of Ius Chasma, Valles Marineris, Mars. J. Maps 13, 260–269. https://doi.org/10.1080/17445647.2017.1296790.

Dohm, J.M., Tanaka, K.L., 1999. Geology of the Thaumasia region, Mars: plateau development, valley origins, and magmatic evolution. Planet. Space Sci. 47, 411–431. https://doi.org/10.1016/S0032-0633(98)00141-X.

Flahaut, J., Quantin, C., Allemand, P., Thomas, P., Le Deit, L., 2010. Identification, distribution and possible origins of sulfates in Capri Chasma (Mars), inferred from CRISM data. J. Geophys. Res. 115, E11007 https://doi.org/10.1029/2009JE003566.

Flahaut, J., Martinot, M., Bishop, J.L., Davies, G.R., Potts, N.J., 2017. Remote sensing and in situ mineralogic survey of the Chilean salars: an analog to Mars evaporate deposits? Icarus 282, 152–173. https://doi.org/10.1016/j.icarus.2016.09.041.

Flahaut, J., Bishop, J.L., Silvestro, S., Tedesco, D., Daniel, I., Loizeau, D., 2019. The Italian Solfatara as an analog for Mars fumarolic alteration. Am. Mineral. 104, 1565–1577. https://doi.org/10.2138/am-2019-6899.

Fueten, F., Flahaut, J., Stesky, R., Hauber, E., Rossi, A.P., 2014. Stratigraphy and mineralogy of Candor Mensa, west Candor Chasma, Mars: Insights into the geologic history of Valles Marineris: Geology of Candor Mensa. J. Geophys. Res. Planets 119, 331–354. https://doi.org/10.1002/2013JE004557.

Fueten, F., Novakovic, N., Stesky, R., Flahaut, J., Hauber, E., Rossi, A.P., 2017. The evolution of Juventae Chasma, Valles Marineris, Mars: Progressive Collapse and Sedimentation: The Evolution of Juventae Chasma. J. Geophys. Res. Planets 122, 2223–2249. https://doi.org/10.1002/2017JE005334.

Gendrin, A., Mangold, N., Bibring, J.-P., Langevin, Y., Gondet, B., Poulet, F., Bonello, G., Quantin, C., Mustard, J., Arvidson, R., LeMouélic, S., 2005. Sulfates in Martian layered terrains: the OMEGA/Mars express view. Science 307, 1587–1591. https://doi.org/10.1126/science.1109087.

Head, J.W., Greeley, R., Golombek, M.P., Hartmann, W.K., Hauber, E., Jaumann, R., Masson, P., Neukum, G., Nyquist, L.E., Carr, M.H., 2001. Geological processes and evolution. Space Sci. Rev. 96, 263–292. https://doi.org/10.1023/A:1011953424736.

Itoh, Yuki, Parente, Mario, 2021. A new method for atmospheric correction and de-noising of CRISM hyperspectral data. Icarus 354, 114024.

Kaplan, H.H., Milliken, R.E., Fernández-Remolar, D., Amils, R., Robertson, K., Knoll, A. H., 2016. Orbital evidence for clay and acidic sulfate assemblages on Mars based on mineralogical analogs from Rio Tinto, Spain. Icarus 275, 45–64. https://doi.org/10.1016/j.icarus.2016.03.019.

Le Deit, L., Flahaut, J., Quantin, C., Hauber, E., Mège, D., Bourgeois, O., Gurgurewicz, J., Massé, M., Jaumann, R., 2012. Extensive surface pedogenic alteration of the Martian Noachian crust suggested by plateau phyllosilicates around Valles Marineris: Plateau Phyllosilicates, Mars. J. Geophys. Res. 117 https://doi.org/10.1029/2011JE003983 n/a-n/a.

Lucchitta, B.K., Bertolini, M.L., 1990. Interior structures of Valles Marineris, Mars. In: Presented at the Lunar Planet. Sci., XX, pp. 590–591.

Lucchitta, B.K., Isbell, N.K., Howington-Kraus, A., 1994. Topography of Valles Marineris: implications for erosional and structural history. J. Geophys. Res. 99, 3783. https://doi.org/10.1029/93JE03095.

Madejová, J., Bednarikova, E., Komadel, P., Cicel, B., 1990. Structural study of acid-treated smectites by IR spectrscopy. In: Presented at the 11th Conf. On Clay Mineralogy and Petrology, Budejovice, pp. 267–271.

Madejová, J., Andrejkovičová, S., Bujdák, J., Čeklovský, A., Hrachová, J., Valúchová, J., Komadel, P., 2007. Characterization of products obtained by acid leaching of Fe-bentonite. Clay Miner. 42, 527–540. https://doi.org/10.1180/claymin.2007.042.4.09.

Madejová, J., Pentrák, M., Pálková, H., Komadel, P., 2009. Near-infrared spectroscopy: a powerful tool in studies of acid-treated clay minerals. Vib. Spectrosc. 49, 211–218. https://doi.org/10.1016/j.vibspec.2008.08.001.

McEwen, A.S., Eliason, E.M., Bergstrom, J.W., Bridges, N.T., Hansen, C.J., Delamere, W. A., Grant, J.A., Gulick, V.C., Herkenhoff, K.E., Keszthelyi, L., Kirk, R.L., Mellon, M.T., Squyres, S.W., Thomas, N., Weitz, C.M., 2007. Mars Reconnaissance Orbiter's high resolution Imaging science experiment (HiRISE). J. Geophys. Res. 112 https://doi.org/10.1029/2005JE002605. E05S02.

Metz, J., Grotzinger, J., Okubo, C., Milliken, R., 2010. Thin-skinned deformation of sedimentary rocks in Valles Marineris, Mars. J. Geophys. Res. 115, E11004 https://doi.org/10.1029/2010JE003593.

Murchie, S.L., Arvidson, R., Bedini, P., Beisser, K., Bibring, J.-P., Bishop, J., Boldt, J., Cavender, P., Choo, T., Clancy, R.T., Darlington, E.H., Des Marais, D., Espiritu, R., Fort, D., Green, R., Guinness, E., Hayes, J., Hash, C., Heffernan, K., Hemmler, J., Heyler, G., Humm, D., Hutcheson, J., Izenberg, N., Lee, R., Lees, J., Lohr, D., Malaret, E., Martin, T., McGovern, J.A., McGuire, P., Morris, R., Mustard, J., Pelkey, S., Rhodes, E., Robinson, M., Roush, T., Schaefer, E., Seagrave, G., Seelos, F., Silverglate, P., Slavney, S., Smith, M., Shyong, W.-J., Strohbehn, K., Taylor, H., Thompson, P., Tossman, B., Wirzburger, M., Wolff, M., 2007. Compact Reconnaissance Imaging Spectrometer for Mars (CRISM) on Mars Reconnaissance Orbiter (MRO). J. Geophys. Res. 112 https://doi.org/10.1029/2006JE002682. E05S03.

Murchie, S.L., Mustard, J.F., Ehlmann, B.L., Milliken, R.E., Bishop, J.L., McKeown, N.K., Noe Dobrea, E.Z., Seelos, F.P., Buczkowski, D.L., Wiseman, S.M., Arvidson, R.E., Wray, J.J., Swayze, G., Clark, R.N., Des Marais, D.J., McEwen, A.S., Bibring, J.-P., 2009a. A synthesis of Martian aqueous mineralogy after 1 Mars year of observations from the Mars Reconnaissance Orbiter. J. Geophys. Res. 114 https://doi.org/10.1029/2009JE003342. E00D06.

Murchie, S.L., Roach, L., Seelos, F., Milliken, R., Mustard, J., Arvidson, R., Wiseman, S., Lichtenberg, K., Andrews-Hanna, J., Bishop, J., Bibring, J.-P., Parente, M., Morris, R., 2009b. Evidence for the origin of layered deposits in Candor Chasma, Mars, from mineral composition and hydrologic modeling. J. Geophys. Res. 114 https://doi.org/10.1029/2009JE003343. E00D05.

Mustard, J.F., Murchie, S.L., Pelkey, S.M., Ehlmann, B.L., Milliken, R.E., Grant, J.A., Bibring, J.-P., Poulet, F., Bishop, J., Dobrea, E.N., Roach, L., Seelos, F., Arvidson, R. E., Wiseman, S., Green, R., Hash, C., Humm, D., Malaret, E., McGovern, J.A., Seelos, K., Clancy, T., Clark, R., Marais, D.D., Izenberg, N., Knudson, A., Langevin, Y., Martin, T., McGuire, P., Morris, R., Robinson, M., Roush, T., Smith, M., Swayze, G., Taylor, H., Titus, T., Wolff, M., 2008. Hydrated silicate minerals on Mars observed by the Mars reconnaissance orbiter CRISM instrument. Nature 454, 305–309. https://doi.org/10.1038/nature07097.

Noel, A., Bishop, J.L., Al-Samir, M., Gross, C., Flahaut, J., McGuire, P.C., Weitz, C.M., Seelos, F., Murchie, S., 2015. Mineralogy, morphology and stratigraphy of the light-toned interior layered deposits at Juventae Chasma. Icarus 251, 315–331. https://doi.org/10.1016/j.icarus.2014.09.033.

Perrin, S., Bishop, J.L., Parker, W.G., King, S.J., Lafuente, B., 2018a. Mars evaporite analog site containing jarosite and gypsum at Sulfate Hill, Painted Desert, AZ. In: 49th Lunar and Planetary Science Conference. The Woodlands, TX.

Perrin, S.L., Bishop, J.L., Parker, W.G., King, S.J., Lafuente, B., 2018b. Mars Evaporite analog site containing Jarosite and gypsum at Sulfate Hill, Painted Desert, AZ. In: Presented at the 49th Annual Lunar and Planetary Science Conference, Woodlands, TX.

Roach, L.H., Mustard, J.F., Murchie, S.L., Bibring, J.-P., Forget, F., Lewis, K.W., Aharonson, O., Vincendon, M., Bishop, J.L., 2009. Testing evidence of recent hydration state change in sulfates on Mars. J. Geophys. Res. 114 https://doi.org/10.1029/2008JE003245. E00D02.

Roach, L.H., Mustard, J.F., Swayze, G., Milliken, R.E., Bishop, J.L., Murchie, S.L., Lichtenberg, K., 2010. Hydrated mineral stratigraphy of Ius Chasma, Valles Marineris. Icarus 206, 253–268. https://doi.org/10.1016/j.icarus.2009.09.003.

Sánchez-Juny, M., Triadú, A., Andreu, A., Bladé, E., 2019. Hydrodynamic determination of the kinematic viscosity of waste brines. ACS Omega 4, 20987–20999. https://doi.org/10.1021/acsomega.9b02164.

Saranathan, A.M., Parente, M., 2021. Adversarial feature learning for improved mineral mapping of CRISM data. Icarus 355, 114107. https://doi.org/10.1016/j.icarus.2020.114107.

Schultz, Richard A., 1998. Multiple-process origin of Valles Marineris basins and troughs, Mars. Planet. Space Sci. 46 (6–7), 827–829.

Scott, D.H., Tanaka, K.L., 1986. Geologic Map of the Western Equatorial Region of Mars.

Seelos, F.P., Seelos, K.D., Murchie, S.L., Novak, M.A.M., Hash, C.D., Morgan, M.F., Arvidson, R.E., Aiello, J., Bibring, J.-P., Bishop, J.L., Boldt, J.D., Boyd, A.R., Buczkowski, D.L., Chen, P.Y., Clancy, R.T., Ehlmann, B.L., Frizzell, K., Hancock, K. M., Hayes, J.R., Heffernan, K.J., Humm, D.C., Itoh, Y., Ju, M., Kochte, M.C., Malaret, E., McGovern, J.A., McGuire, P., Mehta, N.L., Moreland, E.L., Mustard, J.F., Nair, A.H., Núñez, J.I., O'Sullivan, J.A., Packer, L.L., Poffenbarger, R.T., Poulet, F., Romeo, G., Santo, A.G., Smith, M.D., Stephens, D.C., Toigo, A.D., Viviano, C.E., Wolff, M.J., 2023. The CRISM investigation in Mars orbit: overview, history, and delivered data products. Icarus 115612. https://doi.org/10.1016/j.icarus.2023.115612.

Sivasankari, T., Arivazhagan, S., 2022. An analysis of morphology and diverse mineralogy in Ius Chasma, Valles Marineris using MCC, CRISM and CTX Data. J. Indian Soc. Remote Sens. https://doi.org/10.1007/s12524-022-01609-5.

Spencer, R.J., 2000. Sulfate minerals in Evaporite deposits. Rev. Mineral. Geochem. 40, 173–192. https://doi.org/10.2138/rmg.2000.40.3.

Story, S., Bowen, B.B., Benison, K.C., Schulze, D.G., 2010. Authigenic phyllosilicates in modern acid saline lake sediments and implications for Mars. J. Geophys. Res. 115, E12012 https://doi.org/10.1029/2010JE003687.

Tanaka, K.L., 1986. The stratigraphy of Mars. J. Geophys. Res. 91, E139 https://doi.org/10.1029/JB091iB13p0E139.

Tanaka, K.L., Golombek, M.P., Banerdt, W.B., 1991. Reconciliation of stress and structural histories of the Tharsis region of Mars. J. Geophys. Res. 96, 15617–15633. https://doi.org/10.1029/91JE01194.

Thollot, P., Mangold, N., Ansan, V., Le Mouélic, S., Milliken, R.E., Bishop, J.L., Weitz, C. M., Roach, L.H., Mustard, J.F., Murchie, S.L., 2012. Most Mars minerals in a nutshell: Various alteration phases formed in a single environment in Noctis Labyrinthus: Alteration phases in noctis labyrinthus. J. Geophys. Res. 117 https://doi.org/10.1029/2011JE004028 n/a-n/a.

Usabal, G., Bishop, J.L., Danielsen, J.M., Itoh, Y., Parente, M., Seelos, F.P., 2019. Characterization of Jarosite-bearing outcrops northwest of Mwarth Valles. In: Presented at the 50th Lunar Planet. Sci. Conf, The Woodlands, TX.

Viviano, C.E., Seelos, F.P., Murchie, S.L., Kahn, E.G., Seelos, K.D., Taylor, H.W., Taylor, K., Ehlmann, B.L., Wiseman, S.M., Mustard, J.F., Morgan, M.F., 2014. Revised CRISM spectral parameters and summary products based on the currently detected mineral diversity on Mars. J. Geophys. Res. Planets 119, 1403–1431. https://doi.org/10.1002/2014JE004627.

Weitz, C.M., Bishop, J.L., 2016. Stratigraphy and formation of clays, sulfates, and hydrated silica within a depression in Coprates Catena, Mars: Hydrated deposits in coprates catena. J. Geophys. Res. Planets 121, 805–835. https://doi.org/10.1002/2015JE004954.

Weitz, C.M., Milliken, R.E., Grant, J.A., McEwen, A.S., Williams, R.M.E., Bishop, J.L., Thomson, B.J., 2010. Mars reconnaissance orbiter observations of light-toned layered deposits and associated fluvial landforms on the plateaus adjacent to Valles Marineris. Icarus 205, 73–102. https://doi.org/10.1016/j.icarus.2009.04.017.

Weitz, C.M., Bishop, J.L., Thollot, P., Mangold, N., Roach, L.H., 2011. Diverse mineralogies in two troughs of Noctis Labyrinthus, Mars. Geology 39, 899–902. https://doi.org/10.1130/G32045.1.

Weitz, C.M., Noe Dobrea, E.Z., Lane, M.D., Knudson, A.T., 2012. Geologic relationships between gray hematite, sulfates, and clays in Capri Chasma: gray hematite in capri chasma. J. Geophys. Res. 117 https://doi.org/10.1029/2012JE004092 n/a-n/a.

Weitz, C.M., Noe Dobrea, E., Wray, J.J., 2015. Mixtures of clays and sulfates within deposits in western Melas Chasma, Mars. Icarus 251, 291–314. https://doi.org/10.1016/j.icarus.2014.04.009.

Zhang, Mingyang, Gong, Maoguo, Yishun, Mao, Li, Jun, 2018. Unsupervised Feature Extraction in Hyperspectral Images Based on Wasserstein Generative Adversarial Network. IEEE Transac. Geosci. Remote Sens. 99, 1–20.